Hard x-ray nanofocusing by refractive lenses of constant thickness

F. Seiboth, M. Scholz, J. Patommel, R. Hoppe, F. Wittwer, J. Reinhardt, J. Seidel, M. Knaut, A. Jahn, K. Richter, J. W. Bartha, G. Falkenberg, and C. G. Schroer

Citation: Applied Physics Letters **105**, 131110 (2014); doi: 10.1063/1.4896914
View online: http://dx.doi.org/10.1063/1.4896914
View Table of Contents: http://scitation.aip.org/content/aip/journal/apl/105/13?ver=pdfcov
Published by the AIP Publishing

Hard x-ray nanofocusing by refractive lenses of constant thickness

F. Seiboth,[1,a)] M. Scholz,[1] J. Patommel,[1] R. Hoppe,[1] F. Wittwer,[1] J. Reinhardt,[1,2] J. Seidel,[3] M. Knaut,[4] A. Jahn,[4] K. Richter,[4] J. W. Bartha,[4] G. Falkenberg,[2] and C. G. Schroer[1,2,5]
[1]*Institute of Structural Physics, Technische Universität Dresden, D-01062 Dresden, Germany*
[2]*Deutsches Elektronen-Synchrotron DESY, D-22607 Hamburg, Germany*
[3]*Faculty of Mathematics, Technische Universität Chemnitz, D-09107 Chemnitz, Germany*
[4]*Institute of Semiconductors and Microsystems, Technische Universität Dresden, D-01062 Dresden, Germany*
[5]*Department Physik, Universität Hamburg, Luruper Chaussee 149, D-22761 Hamburg, Germany*

(Received 7 July 2014; accepted 16 September 2014; published online 1 October 2014)

In order to focus light or x rays, the thickness of a refractive lens is typically varied over its aperture. Here, we present a refractive x-ray lens made of lamellae of constant thickness, the refractive lamellar lens. Refractive power is created by a specific bending of the lamellae rather than by a concave lens profile. This very special design has the technological advantage that materials like sapphire or diamond can be used to make lenses by coating techniques. A first lens prototype focused x rays with a photon energy $E = 15.25$ keV to a lateral beam size of 164 nm × 296 nm full width at half maximum.
[http://dx.doi.org/10.1063/1.4896914]

To understand the function of nanoscale objects or nano-structured materials, such as organelles in their cellular environment, catalytic nano particles in industrial catalysts, or nano-electronic devices, it is crucial to understand their structure. Hard x-ray microscopy is ideally suited for this type of structure determination in terms of elemental composition,[1] chemical state,[2] and local atomic structure[3] with minimal sample preparation and inside of special sample environments, such as microfluidic cells[4] or chemical reactors.[5]

The spatial resolution in x-ray microscopy is often limited by the x-ray optics. In parallel with the emergence of ever more brilliant x-ray sources over the last two decades, a variety of x-ray optics for imaging and nano-focusing has been developed based on reflection,[6] diffraction,[7] and refraction.[8–11]

In this letter, we present the refractive lamellar lens (RLL). It consists of a set of lamellae of constant thickness that are shaped to generate a parabolic transmission profile in one dimension (cf. Fig. 1). X-ray optically, they are equivalent to conventional parabolic nanofocusing refractive x-ray lenses.[9,10] The unusual lens shape, however, is of a simple elegance and, therefore, has fundamental technological advantages: it allows the use of x-ray optically favorable lens materials, such as sapphire or diamond. For both these materials, nano-structuring tools, such as deep reactive ion etching, are not as advanced as for silicon.[12] Therefore, conventional refractive lenses can currently not be made out of these materials with sufficient quality to allow for nanofocusing. As a result of the lamellar structure, diamond and aluminum oxide can be deposited as films of homogeneous thickness, e.g., by atomic layer deposition (ALD). This opens the way to making nano-focusing lenses of these materials with higher transmission and numerical aperture, generating smaller and more intensive x-ray nano beams.

We made a first prototype shown in Fig. 1, defining the shape of the lamellar structures by deep etching into silicon and subsequent homogeneous coating of the lamellar structures by aluminum oxide (Al_2O_3). Compared to a conventional lens only made of silicon, this optic has a reduced attenuation at increased refractive power. Thus, the numerical aperture and the transmission are improved, increasing the focused flux inside a reduced diffraction limited spot size.

Conventional refractive hard x-ray optics are very similar to lenses used for visible light. Refraction in the lens material focuses the incident beam. For x rays, the index of refraction can be written as $n = 1 - \delta + i\beta$, where the refractive index decrement δ is typically very small ($\sim 10^{-6}$) and positive. Therefore, a focusing lens has to be concave. The weak refraction is compensated by a strong curvature of the lens surfaces and by stacking many single lenses behind

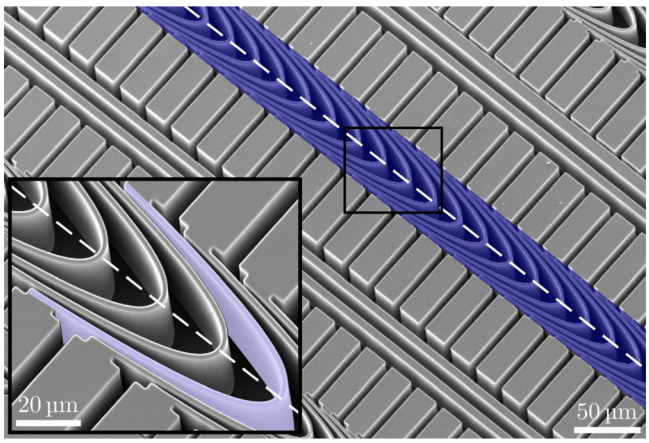

FIG. 1. SEM image of a one-dimensionally focusing silicon RLL coated with Al_2O_3. A single lamella highlighted in the inset is 1.5 µm thick and shaped to form a concave parabolic transmission profile. The whole lens stack (highlighted) is etched 40 µm deep. The optical axis z is marked by the dashed line.

[a)]Electronic mail: frank.seiboth@tu-dresden.de

each other. In paraxial approximation, the thickness $\Delta(r)$ of an ideal aspherical lens is parabolic and for a lens with one curved surface (Fig. 2)

$$\Delta(r) = \frac{r^2}{2R} + d\,.$$

Here, R is the curvature radius and d the thickness at the apex of the parabola $\Delta(r)$.[8] The attenuation inside the lens material limits the transmission, and the effective aperture D_{eff} is thus smaller than the geometric aperture.[8] The diffraction limited focal spot size d_t is determined by Abbe's formula for a Gaussian Airy disk

$$d_t = \alpha\,\frac{\lambda}{2NA} = \alpha\,\frac{\lambda f}{D_{\text{eff}}}\,,$$

with $\alpha = 2\sqrt{2\ln 2}/\pi \approx 0.75$.[8] The numerical aperture is defined by $NA := D_{\text{eff}}/(2f)$, where f is the focal length.[8] Minimization of the diffraction limit d_t is achieved by reducing the focal length f and using a lens material with low atomic number and high density ρ.[9,13] Therefore, nanofocusing lenses made of diamond or sapphire are advantageous.

Here, a single lens is made of a lamella of constant material thickness d. It has to be curved in a specific way, so that the projected thickness $\Delta(r)$ of the lamella along the optical axis has a parabolic profile (cf. Fig. 2). To calculate its shape, the two surfaces of the single lamella are described by the two functions $g(r)$ and $\tilde{g}(r)$, respectively. The shape of the lamella leading to a parabolic transmission profile is given by $g(r) = \tilde{g}(r) + \Delta(r)$ (Fig. 2). To obtain a lamella with constant thickness d, the minimal distance between g and $\tilde{g}$ is required to have the fixed value d. On the optical axis $g'(0)$ is set to zero and hence $g(0) = d$. The shortest distance from any given point $\tilde{P}(\tilde{r}|\tilde{g}(\tilde{r}))$ on $\tilde{g}$ to g is given by the orthogonal projection from $\tilde{P}$ onto g, which is marked by $P(r|g(r))$ in Fig. 2. This can be expressed as

$$\begin{pmatrix} \tilde{r} \\ \tilde{g}(\tilde{r}) \end{pmatrix} = \begin{pmatrix} r \\ g(r) \end{pmatrix} + \frac{d}{\sqrt{1+g'^2(r)}} \begin{pmatrix} g'(r) \\ -1 \end{pmatrix}.$$

Abbreviating $\sqrt{1+g'^2(r)}$ by $e_g(r)$ and using $g(r) - \tilde{g}(r) = \Delta(r)$, one can derive the nonlinear differential equation

$$g(r) - \frac{d}{e_g(r)} = g\left(r + d\,\frac{g'(r)}{e_g(r)}\right) - \Delta\left(r + d\,\frac{g'(r)}{e_g(r)}\right) \qquad (1)$$

that can be solved numerically.

Similar to conventional refractive lenses, the lamellae are stacked behind each other (cf. Fig. 1) to create a strongly focused hard x-ray beam. The curved shape of a single lamella depends only on the thickness d of a lamella and the effective R that should be obtained in projection [cf. Eq. (1)]. The shape for an RLL with $d = 1.5\,\mu\text{m}$ and $R = 20\,\mu\text{m}$ is shown in Fig. 1. When d is decreased while keeping R fixed the lamellae have to be more strongly curved. If d stays constant a smaller R will result in stronger bending of the lamellae.

The above derivations hold for lamellae made of a single material, but can be generalized to coated lamellae made of different materials. For the prototype lenses (Fig. 1) made of Al_2O_3-coated silicon, the shape error introduced by assuming a single lens material and applying Eq. (1) to determine the shape of the compound material is marginal for the special case presented here.[14]

We produced first RLL prototypes for focusing in a crossed geometry at a photon energy of $E = 15.25$ keV, calculating the shape according to Eq. (1). To achieve a point focus, vertically and horizontally focusing RLLs are aligned behind each other. The vertically focusing lens consists of $N = 200$ single lamellae with an effective radius of curvature $R = 20$ μm and a spacing between individual lamellae of $l = 25$ μm, resulting in an overall lens length of $L = Nl = 5$ mm. The second horizontally focusing lens has $N = 260$ lamellae, an overall length $L = 6.5$ mm, and otherwise similar parameters.

The lamellae were coated with aluminum oxide using ALD. A schematic cross-section through a single lamella is shown in Fig. 3 for different fabrication stages. The initial shape calculations were made for a homogeneous lamella with thickness $d = 1.5\,\mu\text{m}$ [Fig. 3(a)]. In the first fabrication step, silicon lamellae were structured into a Si wafer by deep reactive ion etching. They were made thinner than the design thickness, leaving room for a layer of Al_2O_3 [Fig. 3(b)]. The high aspect-ratio lamellae were coated by ALD-Al_2O_3,[15] resulting in a sandwiched lamella profile [Fig. 3(c)]. The final structure consists of a silicon core with $d_{\text{Si}} = 700\,\text{nm}$ and an aluminum oxide layer of $d_{\text{Al}_2\text{O}_3} = 400\,\text{nm}$ on each side,

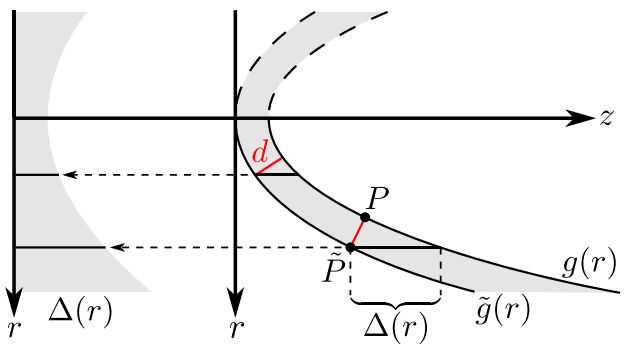

FIG. 2. The parabolic phase shift of a focusing x-ray lens is generated in projection by a lamella of constant thickness d. Its shape, defined by the two functions $g(r)$ and $\tilde{g}(r)$, is chosen to generate a projected thickness $\Delta(r)$ that grows parabolically with r.

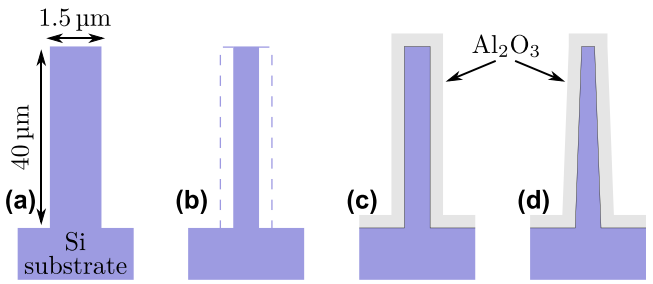

FIG. 3. Schematic cross-section along the optical axis z through a single lens lamella. (a) The design is made for an RLL made of silicon. (b) A thinner silicon scaffold of the lamella is fabricated and (c) coated with Al_2O_3 to reach the nominal thickness. (d) In practice, the thickness of the Si lamella is slightly depth dependent.

resulting in an overall thickness $d = d_{Si} + 2d_{Al_2O_3} = 1.5\,\mu m$. A density of $\rho_{Al_2O_3} = 3.0\ g/cm^3$ was measured for the aluminum oxide film by x-ray reflectometry. This is expected due to the amorphous epitaxial growth of Al_2O_3 and the temperature dependent embedding of hydroxyl groups $(Al(OH)_x)$.[16]

The nanofocusing lens system (two RLLs in crossed geometry) has a geometric aperture of $40\,\mu m \times 40\,\mu m$ and a transmission of $T = 0.061$ at 15.25 keV. The expected ideal diffraction limited focal spot size d_t for the lens system is calculated to $79\,nm \times 93\,nm$ (horizontal × vertical) full width at half maximum (FWHM). The distance from the exit of the lens system to the focal plane is $w = 30.1$ mm. For a pure Si RLL [$d = d_{Si} = 1.5\,\mu m$, cf. Fig. 3(a)], on the other hand, these parameters are $d_t = 99\,nm \times 116\,nm$, $T = 0.034$, and $w = 34.7$ mm. When depositing diamond instead of sapphire we obtain $d_t = 62\,nm \times 75\,nm$, $T = 0.136$, and $w = 27.7$ mm, illustrating the gain in performance by partly replacing silicon.

In practice, the Si etching process generates slightly slanted side walls and thus a non-uniform thickness profile for the Si core of the lens [Fig. 3(d)]. Deviations from the ideal shape introduce aberrations discussed below.

The RLLs were characterized at the nanoprobe endstation of beamline P06 at PETRA III.[17] The x-ray energy was set to $E = 15.25$ keV by a Si-111 monochromator ($\Delta E/E \sim 10^{-4}$) located 38.5 m from the undulator. RLL optics were positioned 98.2 m downstream of the source and characterized by ptychography. This scanning coherent x-ray diffraction imaging technique allows one to quantitatively retrieve the complex wave field illuminating a test object.[18–20] To this end, the test object, an NTT-AT resolution chart (model: ATN/XRESO-50HC), was placed near the focal plane and raster scanned perpendicularly to the beam in 30×30 steps, covering an area of $2\,\mu m \times 2\,\mu m$. At each position of the scan, a far-field diffraction pattern was recorded by a LAMBDA photon counting detector[21] (pixel size: 55 μm) placed 2.165 m behind the sample. Due to a limited counter depth of 12 bit we accumulated 25 single frames with 0.04 s exposure for each scan point, resulting in a total exposure time of 1 s per scan point. From these data, both the complex illuminating wave field [Fig. 4(a)] and the transmission function of the test object [Fig. 4(b)] can be reconstructed simultaneously. In the sample plane, the illumination is quite extended with side lobes reaching to the edges of the field of view. Therefore, details of the resolution test chart far outside the scanned area are faithfully reconstructed [Fig. 4(b)].

The complex wave field at the sample position can be numerically propagated using the Fresnel-Kirchhoff integral to precisely reconstruct the x-ray beam[22] and to analyze aberrations of the focusing optic.[11,20,23] In this way, the full caustic of the beam can be determined.[24] The horizontal and vertical intensity distributions along the beam are depicted in Figs. 5(a) and 5(b), revealing a slight astigmatism. The intensity distribution in the horizontal focal plane [solid line in Figs. 5(a) and 5(b)] is shown in Fig. 5(d) and the corresponding vertical and horizontal intensity profile in Fig. 5(c). Along the horizontal direction [solid line in Fig. 5(d)], the FWHM focal spot size is 164 nm. In the vertical direction [dashed line in Fig. 5(d)], the beam is defocused and has a width of 296 nm. The central focal spot is surrounded by side

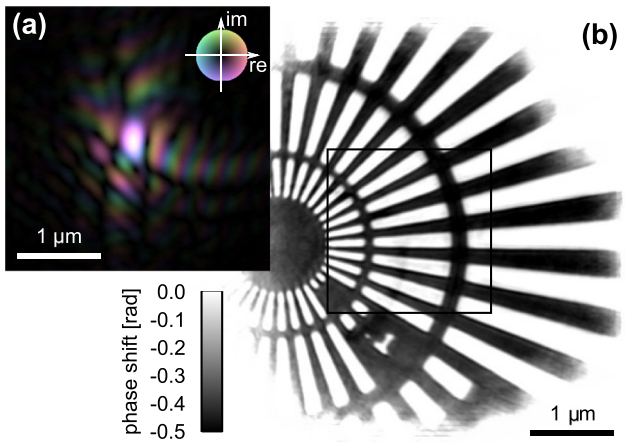

FIG. 4. (a) Ptychographic reconstruction of the illumination at the sample position. Amplitude is encoded by brightness, phase by hue. (b) Reconstruction of the test object. Phase shift is encoded in brightness. The black rectangle in (b) delineates the area scanned by the central speckle.

lobes [cf. Figs. 5(c) and 5(d)], and a splitting of the wave field upstream of the focal plane is observed [cf. Figs. 5(a) and 5(b)]. The astigmatism is a result of a misalignment of the vertically focusing RLL with respect to the horizontally focusing one and is not a property of the optics themselves. The vertical focal plane marked by the dashed line in Fig. 5(b) is located ~3 mm upstream of the horizontal one [solid line in Figs. 5(a) and 5(b)]. In this plane, the vertical spot size is 201 nm FWHM.

Compared to the optimal nominal performance, the first prototype optics generate an increased focal spot size (by about a factor two). The caustic deviates from an ideal Gaussian limited beam: the observed splitting of the beam waist upstream of the focal plane indicates spherical aberrations. SEM images on lamellar test structures showed a non-uniform thickness profile for the etched Si core of a lamella

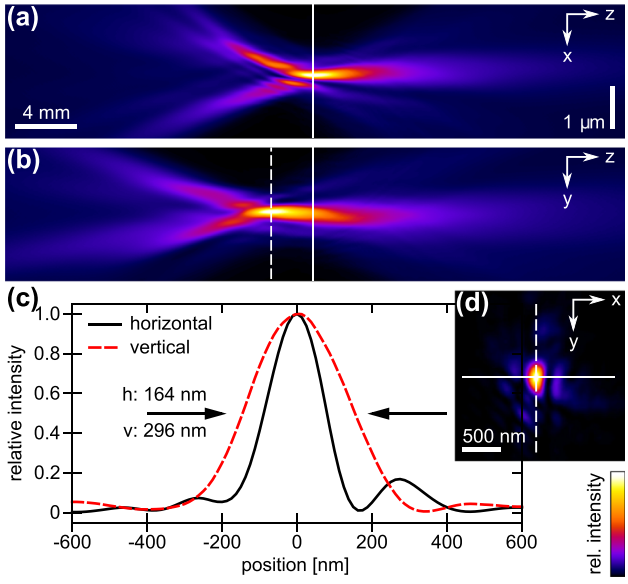

FIG. 5. Propagated wave field for the crossed RLLs. (a) Horizontal intensity distribution along the beam. (b) Beam profile in vertical direction. The vertical focal plane is marked by the dashed line and lies about 3 mm further upstream of the horizontal one marked by the solid line. (c) Intensity profiles in both horizontal and vertical directions, taken from (d). (d) Intensity distribution in the plane marked by the solid line in (a) and (b).

[cf. Fig. 3(d)]. As lamella shape and thickness directly translate to a certain refractive power, the lens shows varying focal distances with etch depth. In addition, these thickness variations introduce deviations from the parabolic transmission profile, as the lamellar shape is only correct for the nominal thickness d. The observed aberrations agree with numerical simulations of the lens and are well understood. A good match of lamella shape and thickness is crucial for aberration-free focusing.

In a next step, RLLs solely made of aluminum oxide are planned by removing the Si core of the lamellae after depositing Al_2O_3. This increases the transmission and numerical aperture and reduces aberrations. Ultimately, an RLL lens system made exclusively of diamond could achieve diffraction limited spot sizes down to 17 nm × 28 nm with a reasonable working distance $w = 5$ mm and transmission up to $T = 0.35$.

This work was supported by the German Ministry of Education and Research (BMBF) under Grant Nos. 05K10OD1 and 05K13OD4 and by VH-VI-403 of the Impuls- und Vernetzungsfonds (IVF) of the Helmholtz Association of German Research Centres. Beamtime at beamline P06 at PETRA III was granted within the user program of DESY, a member of the Helmholtz-Association.

[1]P. Bleuet, L. Lemelle, R. Tucoulou, P. Gergaud, G. Delette, P. Cloetens, J. Susini, and A. Simionovici, "3D chemical imaging based on a third-generation synchrotron source," Trends Anal. Chem. **29**, 518–527 (2010).
[2]J.-D. Grunwaldt, S. Hannemann, C. G. Schroer, and A. Baiker, "2D-mapping of the catalyst structure inside a catalytic microreactor at work: Partial oxidation of methane over Rh/Al_2O_3," J. Phys. Chem. B **110**, 8674–8680 (2006).
[3]P. Bleuet, E. Welcomme, E. Dooryhée, J. Susini, J.-L. Hodeau, and P. Walter, "Probing the structure of heterogeneous diluted materials by diffraction tomography," Nat. Mater. **7**, 468–472 (2008).
[4]S. Köster and T. Pfohl, "X-ray studies of biological matter in microfluidic environments," Mod. Phys. Lett. B **26**, 1230018 (2012).
[5]J.-D. Grunwaldt and C. G. Schroer, "Hard and soft x-ray microscopy and tomography in catalysis: Bridging the different time and length scales," Chem. Soc. Rev. **39**, 4741 (2010).
[6]A. Jarre, C. Fuhse, C. Ollinger, J. Seeger, R. Tucoulou, and T. Salditt, Phys. Rev. Lett. **94**, 074801 (2005); H. Mimura, H. Yumoto, S. Matsuyama, Y. Sano, K. Yamamura, Y. Mori, M. Yabashi, Y. Nishino, K. Tamasaku, T. Ishikawa, and K. Yamauchi, Appl. Phys. Lett. **90**, 051903 (2007).
[7]Y. S. Chu, J. M. Yi, F. De Carlo, Q. Shen, W.-K. Lee, H. J. Wu, C. L. Wang, J. Y. Wang, C. J. Liu, C. H. Wang, S. R. Wu, C. C. Chien, Y. Hwu, A. Tkachuk, W. Yun, M. Feser, K. S. Liang, C. S. Yang, J. H. Je, and G. Margaritondo, Appl. Phys. Lett. **92**, 103119 (2008); H. C. Kang, H. Yan, R. P. Winarski, M. V. Holt, J. Maser, C. Liu, R. Conley, S. Vogt, A. T. Macrander, and G. B. Stephenson, *ibid.* **92**, 221114 (2008); H. Mimura, S. Handa, T. Kimura, H. Yumoto, D. Yamakawa, H. Yokoyama, S. Matsuyama, K. Inagaki, K. Yamamura, Y. Sano, K. Tamasaku, Y. Nishino, M. Yabashi, T. Ishikawa, and K. Yamauchi, Nat. Phys. **6**, 122 (2010); H. Yan, V. Rose, D. Shu, E. Lima, H. C. Kang, R. Conley, C. Liu, N. Jahedi, A. T. Macrander, G. B. Stephenson, M. Holt, Y. S. Chu, M. Lu, and J. Maser, Opt. Express **19**, 15069 (2011); J. Vila-Comamala, S. Gorelick, E. Färm, C. M. Kewish, A. Diaz, R. Barrett, V. A. Guzenko, M. Ritala, and C. David, Opt. Express **19**, 175–184 (2011).
[8]B. Lengeler, C. Schroer, J. Tümmler, B. Benner, M. Richwin, A. Snigirev, I. Snigireva, and M. Drakopoulos, "Imaging by parabolic refractive lenses in the hard x-ray range," J. Synchrotron Radiat. **6**, 1153–1167 (1999).
[9]C. G. Schroer, M. Kuhlmann, U. T. Hunger, T. F. Günzler, O. Kurapova, S. Feste, F. Frehse, B. Lengeler, M. Drakopoulos, A. Somogyi, A. S. Simionovici, A. Snigirev, I. Snigireva, C. Schug, and W. H. Schröder, "Nanofocusing parabolic refractive x-ray lenses," Appl. Phys. Lett. **82**, 1485–1487 (2003).
[10]C. G. Schroer, O. Kurapova, J. Patommel, P. Boye, J. Feldkamp, B. Lengeler, M. Burghammer, C. Riekel, L. Vincze, A. van der Hart, and M. Küchler, "Hard x-ray nanoprobe based on refractive x-ray lenses," Appl. Phys. Lett. **87**, 124103 (2005).
[11]A. Schropp, R. Hoppe, V. Meier, J. Patommel, F. Seiboth, H. J. Lee, B. Nagler, E. C. Galtier, B. Arnold, U. Zastrau, J. B. Hastings, D. Nilsson, F. Uhlén, U. Vogt, H. M. Hertz, and C. G. Schroer, "Full spatial characterization of a nanofocused x-ray free-electron laser beam by ptychographic imaging," Sci. Rep. **3**, 1633 (2013).
[12]B. Nöhammer, J. Hoszowska, A. K. Freund, and C. David, "Diamond planar refractive lenses for third- and forth-generation X-ray sources," J. Synchrotron Radiat. **10**, 168–171 (2003).
[13]C. G. Schroer, F.-E. Brack, R. Brendler, S. Hönig, R. Hoppe, J. Patommel, S. Ritter, M. Scholz, A. Schropp, F. Seiboth, D. Nilsson, J. Rahomäki, F. Uhlén, U. Vogt, J. Reinhardt, and G. Falkenberg, "Hard x-ray nanofocusing with refractive x-ray optics: Full beam characterization by ptychographic imaging," Proc. SPIE **8848**, 884807 (2013).
[14]Replacing Si in parts by Al_2O_3 can result in errors in the transmission profile, since the shape was calculated for a single material with uniform refractive power. However, if the deposition is equal on both sides of the lamella and the overall thickness d of the sandwich corresponds to the design thickness (Figs. 3(a)–3(c)), errors in the parabolic transmission profile are negligible and well within manufacturing tolerances.
[15]M. Knaut, M. Junige, V. Neumann, H. Wojcik, T. Henke, C. Hossbach, A. Hiess, M. Albert, and J. W. Bartha, "Atomic layer deposition for high aspect ratio through silicon vias," Microelectron. Eng. **107**, 80–83 (2013).
[16]M. D. Groner, F. H. Fabreguette, J. W. Elam, and S. M. George, "Low-temperature Al_2O_3 atomic layer deposition," Chem. Mater. **16**, 639–645 (2004).
[17]C. G. Schroer, P. Boye, J. M. Feldkamp, J. Patommel, D. Samberg, A. Schropp, A. Schwab, S. Stephan, G. Falkenberg, G. Wellenreuther, and N. Reimers, "Hard x-ray nanoprobe at beamline P06 at PETRA III," Nucl. Instrum. Methods Phys. Res., Sect. A **616**, 93–97 (2010).
[18]P. Thibault, M. Dierolf, A. Menzel, O. Bunk, C. David, and F. Pfeiffer, "High-resolution scanning x-ray diffraction microscopy," Science **321**, 379–382 (2008).
[19]A. M. Maiden and J. M. Rodenburg, "An improved ptychographical phase retrieval algorithm for diffractive imaging," Ultramicroscopy **109**, 1256–1262 (2009).
[20]A. Schropp, P. Boye, J. M. Feldkamp, R. Hoppe, J. Patommel, D. Samberg, S. Stephan, K. Giewekemeyer, R. N. Wilke, T. Salditt, J. Gulden, A. P. Mancuso, I. A. Vartanyants, E. Weckert, S. Schöder, M. Burghammer, and C. G. Schroer, "Hard x-ray nanobeam characterization by coherent diffraction microscopy," Appl. Phys. Lett. **96**, 091102 (2010).
[21]D. Pennicard, S. Lange, S. Smoljanin, H. Hirsemann, H. Graafsma, M. Epple, M. Zuvic, M.-O. Lampert, T. Fritzsch, and M. Rothermund, "The LAMBDA photon-counting pixel detector," J. Phys.: Conf. Ser. **425**, 062010 (2013).
[22]S. Hönig, R. Hoppe, J. Patommel, A. Schropp, S. Stephan, S. Schöder, M. Burghammer, and C. G. Schroer, "Full optical characterization of coherent x-ray nanobeams by ptychographic imaging," Opt. Express **19**, 16324–16329 (2011).
[23]C. M. Kewish, M. Guizar-Sicairos, C. Liu, J. Qian, B. Shi, C. Benson, A. M. Khounsary, J. Vila-Comamala, O. Bunk, J. R. Fienup, A. T. Macrander, and L. Assoufid, Opt. Express **18**, 23420 (2010); J. Vila-Comamala, A. Diaz, M. Guizar-Sicairos, A. Mantion, C. M. Kewish, A. Menzel, O. Bunk, and C. David, *ibid.* **19**, 21333 (2011).
[24]See supplementary material at http://dx.doi.org/10.1063/1.4896914 for a 3D rendering of the complex wave field.